JOURNAL OF GEOPHYSICAL RESEARCH, VOL. 102, NO. A10, PAGES 22,117–22,130, OCTOBER 1, 1997

Drift-shell splitting of energetic ions injected at pseudo-substorm onsets

Kazue Takahashi,[1,2] Brian J. Anderson,[2] Shin-ichi Ohtani,[2]
Geoff D. Reeves,[3] Shun Takahashi,[4] Theodore E. Sarris,[5,2] and
Kalevi Mursula[6]

Abstract. One feature of a magnetospheric substorm is the injection of energetic particles into closed drift orbits. Injections are routinely observed by geosynchronous satellites and have been used to identify the occurrence of substorms and the local time of particle energization. In this study we examine pitch angle distributions of ion injections in the 50- to 300-keV energy range observed by the Active Magnetospheric Particle Tracer Explorers Charge Composition Explorer (AMPTE/CCE) satellite, hereinafter CCE. In a dipole field, all pitch angles follow the same drift shell, but the day–night asymmetry of the magnetospheric magnetic field introduces a pitch angle dependence in particle drift orbits, so that particles with different pitch angles disperse radially as they drift. The effect is known as drift-shell splitting. For satellite observations near noon at a fixed geocentric distance, the guiding center orbits of ions detected at small pitch angles intersect the midnight meridian at larger geocentric distances than do ions with near-90° pitch angles. The ion pitch angle distributions detected on the dayside therefore provide information about the radial distance of the nightside acceleration region. We apply this principle to study ion injection events observed on September 17-18, 1984, in association with pseudo-substorm onsets. CCE was at 13 hours local time near its apogee (8.8 R_E) and observed a series of ion flux enhancements. Energy dispersion of the timing of the flux increases assures that they are due to injections on the nightside. The flux increases were observed only at pitch angles from 0° to 60°. We calculate drift orbits of protons using the Tsyganenko 89c magnetic field model and find that the drift orbits for 60° pitch angle protons observed at the satellite pass through midnight at 9 R_E, well outside of geostationary orbit, indicating that the ion injections occurred tailward of 9 R_E. Energetic ion data from geostationary satellites for the same time interval show no evidence of injections at 6.6 R_E, consistent with the calculated inner boundary of the injections. Model calculations are presented demonstrating that dispersive injections observed near noon outside geosynchronous orbit provide the greatest sensitivity to drift-shell splitting effects and are therefore most suitable for remote sensing the radial boundaries of substorm injections.

1. Introduction

Sudden enhancements in the fluxes of energetic charged particles in the near-Earth equatorial region are commonly observed in association with magnetospheric substorms. The phenomenon is known as particle injection and is thought to result from sudden acceleration of particles in the near-Earth magnetotail followed by their subsequent drift away from the acceleration region to the observation point(s) [*Konradi*, 1967; *Konradi et al.*, 1975]. Injections have been observed at all local times, and a given injection can be observed at various local times by multiple spacecraft [*Reeves et al.*, 1991]. The acceleration region appears to form an injection boundary [*McIlwain*, 1974; *Lopez et al.*, 1990], and multispacecraft observations have provided information about the azimuthal and radial development of the acceleration region [*Lopez and Lui*, 1990; *Reeves et al.*, 1991].

The injected particles retain information about their acceleration region over many tens of minutes and over large distances as they drift in the magnetospheric magnetic and electric fields. The long memory of the particles is most dramatically exhibited as energy-time dispersion in the arrival time of the particles [*DeForest and McIlwain*, 1971] and as drift echo events [*Brewer et al.*, 1969; *Lanzerotti et al.*, 1971; *Belian et al.*, 1978]. One can infer characteristics of the acceleration region by studying the detailed time development of injections at a given observation point, using the energetic particles to remote sense the acceleration event.

The basic properties of particle drift are well understood in terms of the guiding center theory. For energies below ~50 keV the magnetospheric convection and corotation electric fields play an important role in controlling the particle drift orbits. *Konradi et al.* [1975] reported an example of energy-time dispersion of ions (energy 0–70 keV) observed from the Explorer 45 satellite below L = 5.3. They showed by numerical

[1]Solar-Terrestrial Environment Laboratory, Nagoya University, Toyokawa, Aichi, Japan.
[2]Applied Physics Laboratory, The Johns Hopkins University, Laurel, Maryland.
[3]Los Alamos National Laboratory, Los Alamos, New Mexico.
[4]Power and Industrial R&D Division, Hitachi Ltd., Hitachi, Ibaraki, Japan.
[5]Department of Physics, University of Athens, Athens, Greece.
[6]Department of Physical Sciences, University of Oulu, Oulu, Finland.

Paper number 97JA01870.
0148-0227/97/97JA-01870$09.00

calculation of particle drift orbits that the dispersion can be explained by combining the magnetospheric electric field and the injection boundary proposed by *McIlwain* [1974]. A similar injection boundary has been proposed from the spatial distribution of dispersionless flux enhancements of energetic particles observed by the Active Magnetosphere Particle Tracer Explorers Charge Composition Explorer (AMPTE/CCE, hereinafter CCE) [*Lopez et al.*, 1990].

For particles with sufficiently high energies the drift orbits are determined primarily by the magnetic field configuration. The Earth's dipole field causes electrons to drift eastward and ions to drift westward. The drift speed is proportional to particle energy so that away from the source region, injections at higher energies are observed earlier. This energy dispersion has been used to determine the universal time and local time of injections. One extensively used data source for this analysis is the Los Alamos National Laboratory (LANL) charged particle analyzers (CPA) which measure electrons and ions at energies about 30 keV and higher onboard geostationary satellites [*Belian et al.*, 1978, 1984; *Baker et al.*, 1979; *Reeves et al.*, 1990, 1991]. More recently, a similar technique has been applied to data acquired by the CRRES satellite [*Friedel et al.*, 1996].

In this paper we demonstrate that another property of particle drift, drift-shell splitting, can be used to investigate the source region of the particles, and in particular, the radial extent of the source. Drift-shell splitting is a well known phenomenon which arises from local time asymmetry of the magnetospheric magnetic field. Quantitative analyses of drift-shell splitting were made as early as the 1960s [*Hones,* 1963; *Fairfield*, 1964; *Roederer*, 1967]. Somewhat surprisingly, little has been discussed about drift-shell splitting effects of substorm injections, although pitch angle time dispersion of injection has been noted [*Konradi et al.*, 1975; *Walker et al.*, 1978].

We study injections associated with pseudo-substorm onsets observed on one CCE orbit. The events were chosen primarily because the observed shell splitting effects were especially clear and also because related data from geostationary satellites and ground magnetic field observatories were available. We have found that drift-shell splitting effects are usually observed by CCE during typical substorms but that multiple injections occurring in short intervals for normal substorms produce complicated injection profiles that are difficult to interpret uniquely. Pseudo-substorm onsets, however, display pitch angle effects quite clearly. For the purposes of studying the drift-shell splitting effects per se we therefore focus attention on pseudo-substorm onsets.

The paper is organized as follows. Section 2 describes the relationship between drift-shell splitting and the radial extent of the injection region, showing that the radial extent of the injection region corresponds to a range of pitch angles observed at a given dayside location. Section 3 presents model calculations of proton drift-shell splitting using the T89c magnetic field model [*Tsyganenko*, 1989]. There are noticeable differences between results using guiding center approximation and explicit Lorentz force integration due to the onset of nonadiabatic motion, so we adopt the explicit integration results for comparison with events. Section 4 presents observations and modeling for specific ion injection events on September 17-18, 1984, showing that injected ions are observed only at pitch angles less than 60°, implying that the acceleration region was tailward of about 9 R_E. The implications of the results for future work are discussed in section 5, and the paper is summarized in section 6.

2. Injection Pitch Angle Signatures of Drift-Shell Splitting

We first consider the relationship between the pitch angle of injected ions and the radial distance of the acceleration region. Figure 1, adapted from *Roederer* [1967, Figure 7], illustrates the effects of drift-shell splitting in a time-stationary magnetosphere with no convection electric field. As *Roederer* [1967] noted, it is straightforward to determine which way the equatorial radius of the drift orbit shifts from the dayside to the nightside using the first two adiabatic invariants, that is, the magnetic moment and the parallel action integral.

Consider a field line on the noon meridian which threads a spacecraft located at the equator. The field line is populated by particles with various mirror latitudes. A particle mirroring near the equator, at location A in Figure 1, conserves its magnetic moment by following the orbit on which the equatorial magnetic field magnitude is nearly constant. On the dayside at radial distances of ~5 to ~10 R_E the magnetic field intensity is higher than the dipole value owing to the Chapman-Ferraro magnetopause current. On the nightside the magnetic field for the same distance range is weaker than the dipole value owing to the cross-tail currents. Thus a particle that crosses the noon meridian at $R = R_0$ crosses the midnight meridian at a radial distance smaller than R_0. The mirror point and the associated field line for this particle are labeled A′. A particle that mirrors away from the equator, at location C, on the same $R = R_0$ field line at noon conserves both the mirror point magnetic field in-

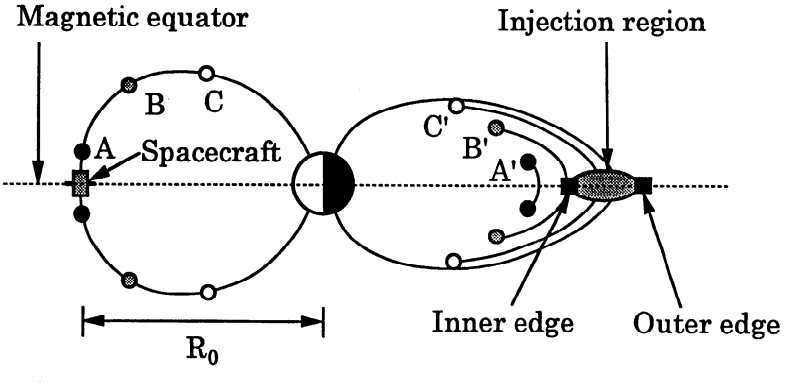

Figure 1. Schematic illustration of drift-shell splitting, adapted from *Roederer* [1967].

tensity, B_m, and the parallel action integral $\int v_{\parallel} ds$ evaluated between the mirror points, where $v_{\parallel}$ is the parallel component of velocity. The conservation of the first invariant is equivalent to conservation of the magnetic field magnitude at the mirror points, and the conservation of the second invariant is approximately equivalent to conservation of the field line length between the northern and southern mirror points. These conditions are satisfied if the particle crosses the nightside at a radial distance greater than R_0. The field line and mirror point for this particle are labeled C′. For a particle mirroring between locations A and C, labeled B, the nightside field line will be located between those for A′ and C′.

These qualitative considerations are consistent with quantitative evaluation of the drift-shell splitting effect based on realistic magnetospheric magnetic field models. For example, *Reeves et al.* [1991] used the *Tsyganenko and Usmanov* [1982] magnetic field model and the guiding center approximation to find that the drift shells of ions starting from the noon meridian at the distance of 6.7 R_E split to a radial distance range of 6.2 to 7.4 R_E on the nightside. To summarize, among particles populating the same field line on the noon meridian, those with higher mirror latitudes cross the midnight meridian at greater distances, and equatorially mirroring particles cross the midnight meridian closer to the Earth.

Now consider the effects of drift-shell splitting on the observed pitch angle distribution of a substorm injection. Assume that an injection takes place in a region represented by the shaded oval in Figure 1 with inner and outer edges as indicated. The duration of the injection as observed at a given pitch angle and energy is determined primarily by the local time extent of the region. Although particle acceleration may take place near the neutral sheet, all field lines threading the injection region will be populated by accelerated particles. Immediately after the injection, the accelerated particles start drifting azimuthally toward the dayside. The key point is that for a given energy, particles arriving at the dayside observation point with different pitch angles necessarily originate from different radial distances in the acceleration region. Conversely, for a given radial distance in the injection region only one pitch angle will reach the satellite.

This implies that the radial extent of the acceleration region corresponds to a finite range of pitch angles observed in the injection. In Figure 1 the field line labeled B′ intersects the inner edge of the injection region, and only those particles on this field line mirroring at B′ are on the drift shell that intersects the satellite. Since these particles mirror at point B on the dayside, the injection on field line B′ will be detected only at pitch angles corresponding to mirror points at B. Particles observed on the dayside that mirror at higher latitudes than B correspond to field lines in the injection region tailward of B′. Thus, if the acceleration region has a sharp inner edge and it intersects one of the nightside drift shells of the particles encountering the dayside satellite, the inner edge will appear as an upper bound on the pitch angles observed in the injection. Conversely, the outer radial edge of the acceleration region corresponds to a lower bound on the pitch angles observed in the injection. Thus by measuring the range of pitch angles appearing on the dayside in a given injection event, one indirectly detects the radial extent of the injection region.

3. Model Calculations of Proton Orbits

To illustrate the correspondence between dayside pitch angle and nightside drift path radial distance, we present model calculations of proton drift orbits. Because the injection region is in the magnetotail where the particle motions can be strongly nonadiabatic, potentially having a significant effect on the drift trajectories [*Anderson et al.*, 1997], we perform explicit integration of the Lorentz force equation in addition to a guiding center integration [cf. *Roederer*, 1967; *Ejiri et al.*, 1980; *Takahashi and Iyemori*, 1989; *Reeves et al.*, 1991]. The technical detail of the explicit integration has been presented elsewhere [*Anderson et al.*, 1997]. Briefly, a particle is launched with specified initial energy, gyrophase, and pitch angle and is traced by numerically integrating the Lorentz equation of motion. As described by *Anderson et al.* [1997], the equatorial plane projection of the drift trajectory is calculated from the motion of a single particle by evaluating the instantaneous particle gyrocenter, given by the particle velocity, Larmor radius, and magnetic field direction, and then tracing the field line threading the gyrocenter to the equatorial plane. For both the guiding center and direct integrations we used the Tsyganenko 1989c magnetic field model [*Tsyganenko*, 1989; *Peredo et al.*, 1993] and the shielded convection electric field model [*Volland*, 1973; *Stern*, 1975] together with a dipole corotation electric field. The onset of nonadiabatic motion agrees with the analytical theory of nonadiabatic motions [*Birmingham*, 1984; *Anderson et al.*, 1997]. The explicit and guiding center integration methods agree where nonadiabatic effects are negligible. For this paper, we consider only protons with energies greater than 50 keV. In section 3.1 we show examples of ion orbits for the T89c (Kp = 2) model without an electric field, and then in section 3.2 examine the effects of varying Kp and including the electric field. Comparisons of runs with and without the electric field indicate that the electric field does not substantially affect the duskside trajectories of the particles.

3.1. Ion Trajectories for the T89c (Kp = 2) Model Without an Electric Field

Despite the nonadiabatic behavior of protons on the nightside one can still uniquely specify the nightside point of origin given the dayside position, energy, and pitch angle by backtracing particle trajectories in time. Protons with energies above about 50 keV and midnight distances of about 6 R_E suffer irreversible pitch angle scattering with each transit through the equator owing to the small field line radius of curvature [*Anderson et al.*, 1997]. Nonetheless, the average drift shell in the nonadiabatic regime remains well defined. As protons drift toward the dayside and the equatorial field line radius of curvature increases, they gradually become adiabatic. Their adiabatic drift paths are determined by the pitch angle they acquire randomly as they emerge from the nonadiabatic regime. Thus a single nonadiabatic nightside drift path fans out into a family of adiabatic drift paths. Because the pitch angle scattering history is extremely sensitive to gyrophase, it is impossible to predict which adiabatic path a given particle will take. However, when viewed backward in time, the family of adiabatic drift paths converge to a single nonadiabatic drift path, so it is possible to assign the midnight position given a dayside position and pitch angle. Thus, despite the nightside nonadiabatic behavior, the dayside pitch angles correspond to nightside points of origin according to the geometric relationship between dayside and nightside drift shells as shown in Figure 1.

Figure 2 illustrates examples of numerically calculated proton drift orbits. For this example we used the Kp = 2 magnetic field model with zero tilt, no electric field, and a proton energy of 200 keV. The traces show the equatorial gyrocenter point as

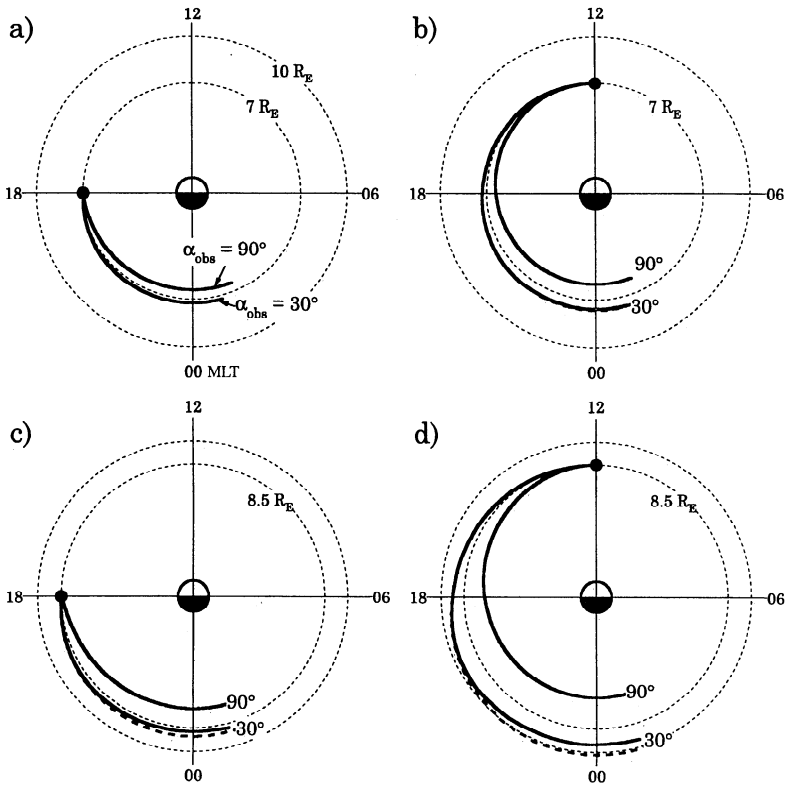

Figure 2. Guiding center orbits of protons arriving at four representative satellite locations (solid dots) with two representative equatorial pitch angles, 30° and 90°. The proton energy is assumed to be 200 keV. Solid traces are results of direct integration of the Lorentz force equation, and dashed traces are results obtained using the guiding center approximation. The two methods differ significantly only for traces from noon at 8.5 R_E.

the proton is traced back from the observation point indicated by a solid dot. The solid traces give the explicitly integrated drift path, and the dashed traces show the guiding center calculation. Time-reversed traces are shown from four observation points: L = 7 near geostationary orbit, L = 8.5 near CCE apogee, and two observed pitch angles, α_{obs} = 30° and 90°, at each point. Nonadiabatic effects produce some random scatter in the nightside drift paths. The scattering is extremely sensitive to initial gyrophase, but the average drift path, defined as an average over the initial gyrophase, remains well defined [*Anderson et al.*, 1997]. The traces shown here are averages of traces of eight particles with evenly spaced initial gyrophases over the range 0° to 360°. Owing to nonadiabatic effects, the actual orbits of particles with α_{obs} smaller than 30° have almost identical drift paths as α_{obs} = 30° particles. The range α_{obs} = 30° to 90° therefore gives the entire spread of drift shells.

In each diagram the separation of the drift orbits between the two α_{obs} values is clear and is qualitatively consistent with Figure 1. That is, the orbit of the α_{obs} = 30° particle is located outside of the orbit of the α_{obs} = 90° particle. Comparing the explicit (solid curves) and guiding center (dashed curves) integrations we see that they are indistinguishable for observation points at geosynchronous orbit but differ by slightly less than 1 R_E at midnight for the noon L = 8.5 observation point. In addition, there are two qualitative points to be made. First, for a given radial distance of a satellite, the radial separation of the drift orbits at midnight, ΔR(24 magnetic local time (MLT)) = R(24 MLT, α_{obs} = 90°) − R(24 MLT, α_{obs} = 30°), is larger when the satellite is located at noon than at dusk. This means that a larger distance range at midnight can be remotely sensed when the satellite is at noon than at dusk. Second, for a given local time of the satellite, ΔR(24 MLT) is larger when the satellite is located at the larger radial distance.

The variations of R(24 MLT) and ΔR(24 MLT) with the local time of observation for satellites at 7 and 8.5 R_E are shown in Figure 3, with the explicit (guiding center) integration results on the left (right). For the explicit method the particle energy was assumed to be 200 keV. The upper panels show the midnight radial distance of particle orbits as a function of the observation point local time, again for two geocentric distances, 7 and 8.5 R_E and for α_{obs} = 30° and 90°. The bottom panels show ΔR at the two radial distances between the α_{obs} = 30° and 90° particles. This figure shows that for both radial observation distances, the α_{obs} = 90° particles cross midnight closer to Earth than the observation point, whereas the α_{obs} = 30° particles cross midnight farther from Earth than the observation point. As the observation local time approaches midnight, the radial displacement of midnight crossing points for particle drift tailward or earthward decreases as it must. The guiding center approximation predicts that α_{obs} = 30° particles drift somewhat farther tailward than given by the explicit integration, consistent with the results of Figure 2. The maximum difference is about 0.8 R_E for observations at 8.5 R_E and noon MLT. Although not large, the effects of nonadiabatic motion of drift are evident, and we therefore use the explicit integration results for the remainder of this paper.

The results show that observations made near noon beyond geosynchronous orbit are the most sensitive to drift-shell split-

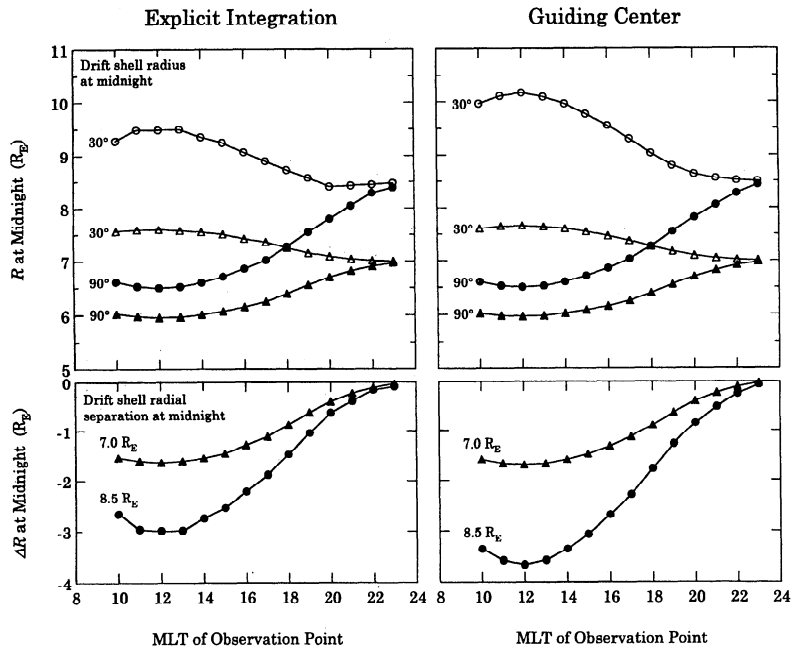

Figure 3. (top) Radial distance of drift orbit at midnight for particles originating from two radial distances $R = 7\ R_E$ (triangles) and $R = 8.5\ R_E$ (circles) with two pitch angles at the observation point, as a function of the initial local time of the particle. (bottom) Radial separation at midnight of drift orbits of particles with two pitch angles as a function of the initial local time of the particle. Left (right) hand panels show explicit Lorentz force (guiding center) integration results. For the explicit method the particle energy is assumed to be 200 keV.

ting effects. The difference in the midnight distances of $\alpha_{obs} = 90°$ and 30° protons is up to 3 R_E for particles observed at 8.5 R_E but about half as large, 1.5 R_E, for particles observed at 7 R_E. At 8.5 R_E, particles observed before 16 MLT have midnight crossing points separated by more than 2 R_E. This shows that dayside observations beyond geosynchronous orbit in the early afternoon sector provide the greatest range of radial distances with pitch angle and that noon is the optimal position, providing the greatest range of radial drift path midnight crossing distances. Moreover, it is possible to detect injection events tailward of 8 R_E only for observations from distances greater than 7 R_E, whereas injections as close as 6.5 R_E remain detectable out to observation radial distances of 8.5 R_E.

3.2. Effects of Varying the Magnetic Field and Including an Electric Field

The model calculation was extended to T89c models for different Kp values with an electrostatic field in the magnetosphere in order to examine how the drift paths might vary according to changes in the geomagnetic condition and also to confirm that the assumption of zero electric field gives a reasonable estimate of the drift-shell radius near midnight. For the variation of the electric field with Kp we use the empirical relation of *Maynard and Chen* [1975] derived for the Volland–Stern electric field [*Volland*, 1973; *Stern*, 1975]. At midnight, noon, and dusk for 8.5 R_E the dawn–dusk (convection) electric field increases from 0.070 mV/m for Kp = 1 to 0.099 mV/m for Kp = 3 and 0.137 mV/m for Kp = 5.

Figure 4 shows the electric field effect on the proton drift paths. As before, the ion orbits were calculated backward in time from the satellite location at noon, 8.5 R_E. When the electric field is included ($E \neq 0$), the orbit depends on particle energy as demonstrated by the three traces representing 50-, 100-, and 200-keV protons. The orbit at 18 MLT is progressively shifted earthward as the energy increases. However, the orbit radial distances in the region of substorm onset, 21 to 24 MLT,

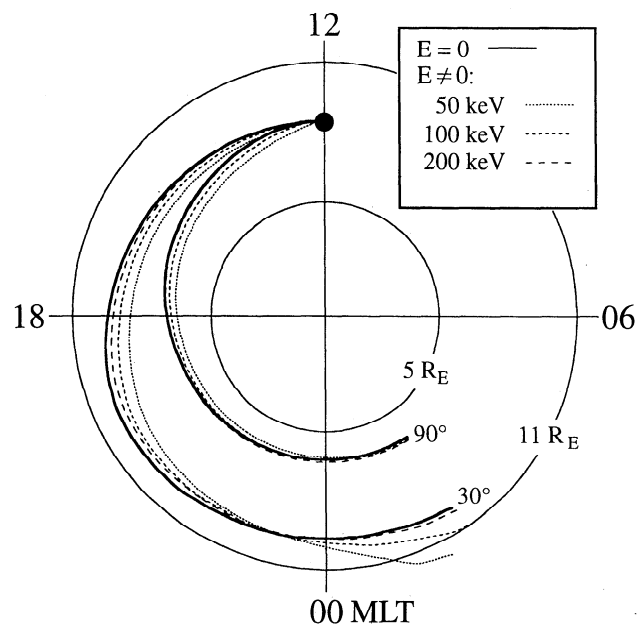

Figure 4. Guiding center drift paths from 03–12 MLT for Kp = 3 field models without an electric field ($E = 0$) and with an electric field ($E \neq 0$) for 50-, 100-, and 200-keV protons.

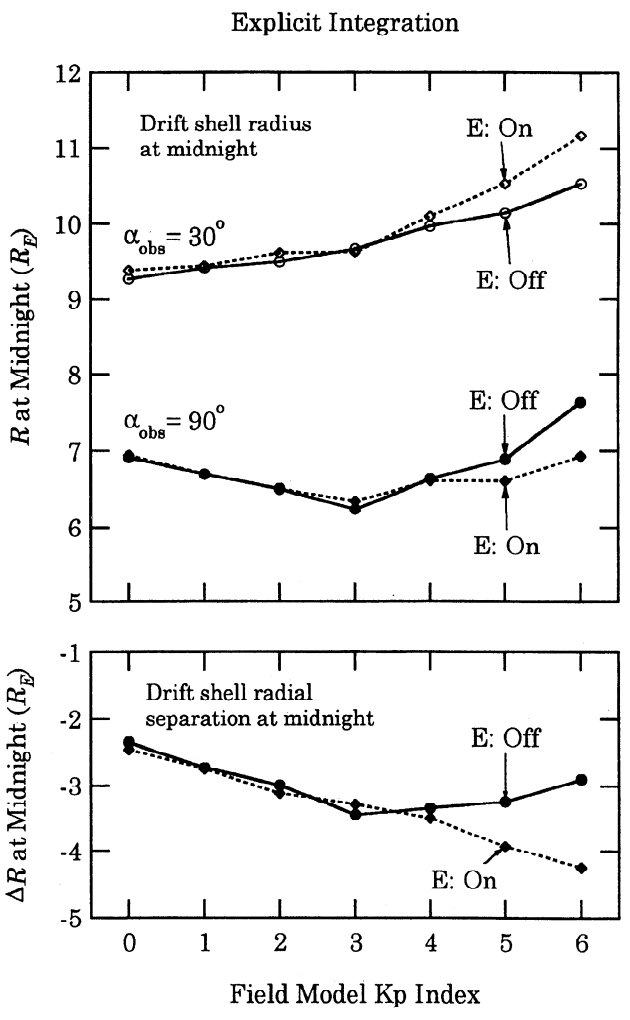

Figure 5. (top) Midnight equatorial distance of the drift path versus *Kp* for 200-keV protons arriving at noon, 8.5 R_E, with equatorial pitch angles (α_{obs}) of 30° and 90°. (bottom) The difference between the midnight equatorial distance of the drift paths for the two pitch angles. Cases with and without an electric field are shown for each pitch angle.

are quite insensitive to particle energy down to 50 keV. The dominant factor governing the radial distance in the substorm onset region is the pitch angle, not the energy. Also, we find that the E = 0 case gives a quite seasonable estimate of the radial distances in the 21 to 24 MLT region.

Figure 5 (top) shows the *Kp* dependence of the midnight radial distance R(24 MLT) of the drift path for the two pitch angles, 30° and 90°. The point of particle observation, noon at 8.5 R_E, is the same as before, and 200-keV protons are used. Cases with and without an electric field are also compared. Because the degree of tailward stretching of the T89c model field increases with *Kp*, the distance R(24 MLT) changes systematically with *Kp*. In the E = 0 case, $R(\alpha_{obs} = 30°)$ increases monotonically from ~9 R_E for *Kp* = 0 to ~10.5 R_E for *Kp* = 6, whereas $R(\alpha_{obs} = 90°)$ is in the range of 6.3 to 7.7 R_E and takes the minimum value at *Kp* = 3. This behavior is largely the same when the electric field is turned on except for a minor (less than 0.7 R_E) difference at large *Kp*. The drift path separation ΔR(24 MLT) shown at the bottom indicates that the separation tends to increase with *Kp* from 2.3 R_E for *Kp* = 0 to 3.4 R_E for *Kp* = 3.

These test particle runs indicate that, although the magnetic field configuration and E control the individual ion drift paths, the radius of the nightside drift path for a given pitch angle does not change much when the electric field is included and that the paths for the two pitch angles are well separated near midnight for a wide range of *Kp*. It is worth noting that the electric field does not affect the ion behavior in the region where pitch angle scattering occurs. Although particles pitch angle scatter so that their drift changes, they do not become demagnetized in the sense that the particles traverse large distances near the equator under the influence of the electric field [*Speiser*, 1965]. For the orbits considered here, for $R < 10\ R_E$, the particles pitch angle scatter when they cross the equator, but they do not display the chaotic behavior typically associated with deeper tail field reversal studies, that is, equator reflections and Speiser orbits.

Finally, we note that we have not incorporated the effect of inductive electric fields. At present we have no handle on the inductive field, because it implies a time-dependent magnetic field. We do not believe there is any reliable time-dependent global model of the magnetic field appropriate for the expansion phase of a substorm. Our objective is to estimate the location of particles immediately after a major acceleration and describe their subsequent motion, not to determine how the particles behaved before or during the acceleration.

4. Observation and Modeling of Ion Injections on September 17-18, 1984

To test whether drift-shell splitting and pitch angle–dependence effects are present in dayside observations of injection events we analyze a series of ion injections observed during a 5-hour interval on September 17-18, 1984. The primary data for this analysis are energetic ion fluxes (assumed to be protons) measured by the ion head of the Medium-Energy Particle Analyzer (MEPA) on CCE [*McEntire et al.*, 1985]. CCE was an elliptically orbiting equatorial satellite with apogee of 8.8 R_E and inclination of 5°. We use ion fluxes measured in five energy bands covering 28 to 320 keV at the time of the observations presented below. The CCE data are supplemented by energetic particle measurements from three geostationary satellites carrying LANL CPAs. All these instruments had the capability of sampling a wide range of pitch angles using satellite spin, but only CCE data will be used to study the pitch angle dependence of ion injections.

4.1. Overview of the Injections

Figure 6 shows the L versus MLT plots of the relevant satellites and ground stations from 2000 UT on September 17 to 0100 UT on September 18. The coordinates are based on an internal magnetic field, so the location of the high-latitude ground station Soroya in this diagram should not be taken as accurately representing the equatorial crossing point of the field line originating from the station. CCE was at geocentric distances greater than 8 R_E for 12–14 MLT. The spacecraft apogee (8.8 R_E) occurred at 13.3 MLT. CCE was close to the dipole equator with dipole latitude changing from 7.5° at 2000 UT to −3.4° at 0100 UT, so the pitch angle at the satellite was essentially the same as the equatorial pitch angle. During the period of interest, coverage at geosynchronous orbit was provided by 1977-007 in the postmidnight sector, 1982-019 in the premidnight sector, and 1984-037 mainly in the postnoon sector.

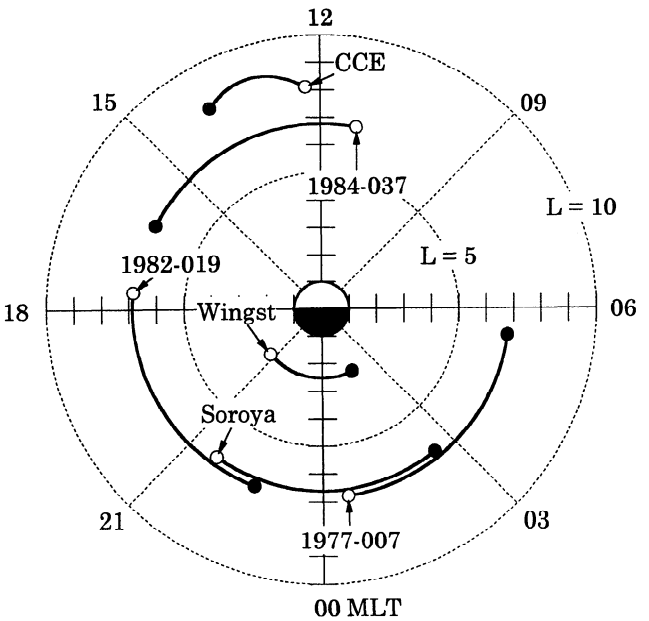

Figure 6. *L* versus MLT (1984, day 261, 2000 UT to day 262, 0100 UT) plot of the location of four satellites and two ground stations for the time interval chosen for analysis of ion injections. The open and closed circles correspond to the beginning and ending of the interval. The magnetic coordinates are based on a centered dipole.

Figure 7 shows a 14-hour summary plot of CCE ion data including the 5-hour interval defined above. The plot is approximately centered on the satellite apogee and covers nearly a full orbit. The traces in the figure represent the number fluxes of energetic ions measured by MEPA in five energy bands. For each energy band, data are averaged in two pitch angle bins, one for 45°–135° (plotted in thin trace and labeled "Perpendicular") and the other for 0°–45° and 135°–180° (plotted in thick trace and labeled "Parallel"). MEPA had a 32-sector angular resolution in the satellite spin plane, and because the spin axis was approximately parallel to the Sun–Earth line, a wide range of pitch angles was covered in regions dominated by the Earth's dipole field. For the event under study the pitch angle coverage was from ~10° to ~170°. The sectored data have time resolutions between ~6 s (one satellite spin) and ~24 s (four spins), and 24-s averages are shown here.

The temporal profiles of the parallel and perpendicular fluxes are significantly different. The parallel fluxes exhibit distinctive enhancements in a 5-hour interval around the spacecraft apogee. If we take the 56- to 92-keV band, for example, flux peaks occur at 2120 2220, 2320, and 0010 UT. Similar peaks are observed in other energy bands at slightly different times, consistent with energy dispersion of ion injections on the nightside. The perpendicular fluxes, by contrast, exhibit a largely smooth variation, reflecting a time-stationary earthward radial density gradient. Fluctuations exist in the perpendicular fluxes, but they are far less pronounced than the variations seen in the parallel fluxes (see section 4.2 for details).

Ion injections occurring only at low pitch angles is a typical feature in the CCE data on many orbits with apogee on the dayside. Since 90° pitch angles almost always dominate the distribution, most of these low pitch angle injections are completely obscured if the data are averaged over all pitch angles. It is only by dividing the data as shown that one can identify these low pitch angle injection events.

The energy dispersion of the flux enhancements indicates that they are not locally produced. In each event the flux maximum occurs earlier at higher energy, indicating that ions were "injected" at a distant location and drifted to the satellite. The most likely location of injection is the near-Earth magnetotail. In this respect the injection events are quite similar to those routinely observed by geostationary satellites. However, since the present events were observed at $L > 8$ and only in the parallel pitch angle bin, they are not exactly analogous to typical geostationary events. One indication of the departure from the typical geostationary observations is that the geomagnetic activity was low during the injection events. For example, *AE* was less than 100 nT from 2000 to 0100 UT. The 3-hour *Kp* values corresponding to this time interval were also low at 1−, 1−, and 0+.

The low *AE* values do not mean that there was no temporal variation in geomagnetic activity. On the contrary, each of the injections was associated with a small change in high-latitude magnetic field and a midlatitude Pi 2 pulsation. Figure 8 shows the northward magnetic field components at Soroya (geomagnetic latitude equal to 66°, local time equal to UT + 1.5 hours) and Wingst (magnetic latitude equal to 54°, local time equal to UT + 0.6 hour) for 2000–0100 UT. The Soroya station is part of the European Incoherent Scatter (EISCAT) magnetometer chain [*Lühr et al.*, 1984]. Wingst data were obtained by a rapid-run magnetometer, so they represent the time derivative of the magnetic field. The Soroya data are characterized by a series of negative perturbations ($|\Delta X| \leq 100$ nT), which implies

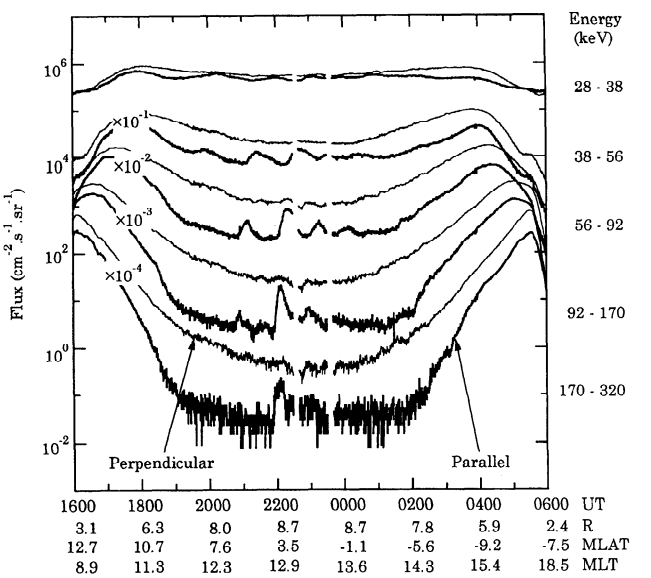

Figure 7. Ion flux in five energy bands measured from CCE on the orbit illustrated in Figure 4 (September 17-18, 1984, days 262-262). In each energy band, fluxes are averaged in two pitch angle bins and are plotted separately. Fluxes are generally higher in the pitch angle bin covering 45°–135° (labeled "Perpendicular"), but short-duration flux enhancements, or injections, are observed only in the pitch angle bin covering 0°–45° and 135°–180° (labeled "Parallel"). There are data gaps at ~2230 and 2330 UT. The satellite location is indicated at the bottom using geocentric distance *R* (Earth radii), dipole latitude MLAT (degrees), and magnetic local time MLT (hours).

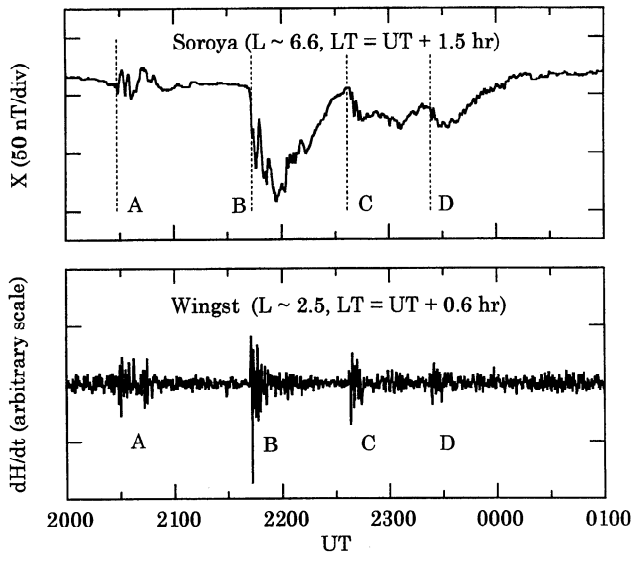

Figure 8. Horizontal magnetic field components at an auroral zone (Soroya) and a midlatitude (Wingst) station for time interval of ion injections shown in Figure 5 (September 17-18, 1984, days 261-262). The Wingst data have been band-pass-filtered to illustrate Pi 2 bursts. Vertical dashed lines indicate the onset of Pi 2 pulsations at Wingst. Four major Pi 2 events are labeled A through D.

minor enhancements of the auroral electrojet. We have also examined the magnetogram from Bear Island (magnetic latitude equal to 71°, magnetic longitude 109°) to infer the location of the electrojet. At this station the H component perturbations for 2000–0100 UT were similar to those observed at Soroya, whereas the Z component perturbations were negative, opposite to those observed at Soroya. From these observations we infer that the electrojet was located between the two stations, possibly at a magnetic latitude of ~69°. In the Wingst data we identify four major Pi 2 pulsations occurring at 2028 UT (event A), 2142 UT (event B), 2237 UT (event C), and 2322 UT (event D). The Pi 2 onset times, indicated by vertical dashed lines in the upper panel, demonstrate that the Pi 2 onset and the decrease in X at Soroya are highly correlated. These consistent behaviors of high-latitude small negative bays and midlatitude Pi 2 pulsations suggest that they are due to pseudo-substorm onsets [*Akasofu*, 1964; *Koskinen et al.*, 1993; *Ohtani et al.*, 1993; *Nakamura et al.*, 1994]. Although the events could just as well be termed weak substorms, we use the term pseudo-substorm onsets throughout this paper to emphasize their morphological difference from fully developed normal substorms and to be consistent with recent studies that used the term "pseudo" [*Koskinen et al.*, 1993; *Ohtani et al.*, 1993; *Nakamura et al.*, 1994].

Figure 9 shows the detail of the flux variations in the parallel pitch angle bin and their relation to Pi 2 pulsations. The symbols above the peaks in each flux trace indicate the Pi 2 onset times plus a constant lag time. The lag time was determined by visually matching the Pi 2 and flux plots. The lag is 56 min for 38–56 keV and decreases to 18 min for 170–320 keV. Because of the broadness of the flux peak, the time lag has an inherent uncertainty of a few minutes, which would translate to an uncertainty in injection local time of ~2 hours. Within this timing uncertainty the time intervals between the flux peaks and the Pi 2 onsets match quite well for each energy. This fact implies that each injection was associated with a Pi 2 pulsation and that the injection local time probably did not change more than 2 hours from events A through D.

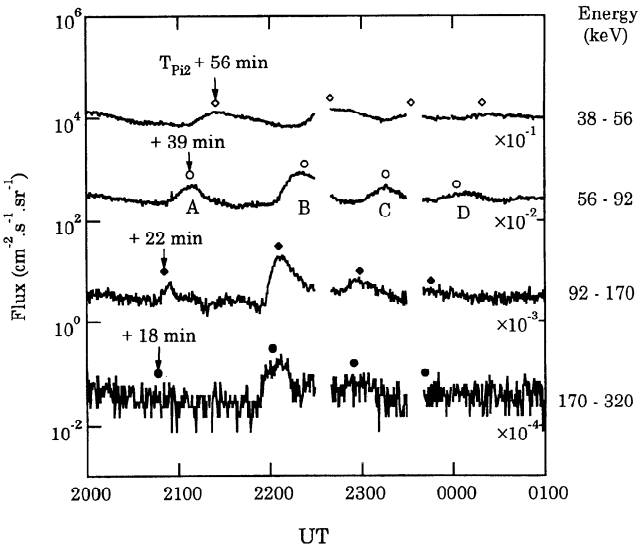

Figure 9. Detail of ion injections observed in the parallel pitch angle bin (September 17-18, 1984, days 261-262). Time delay of flux peak from Pi 2 onset time T_{Pi2} is indicated for the four energy bands using different symbols.

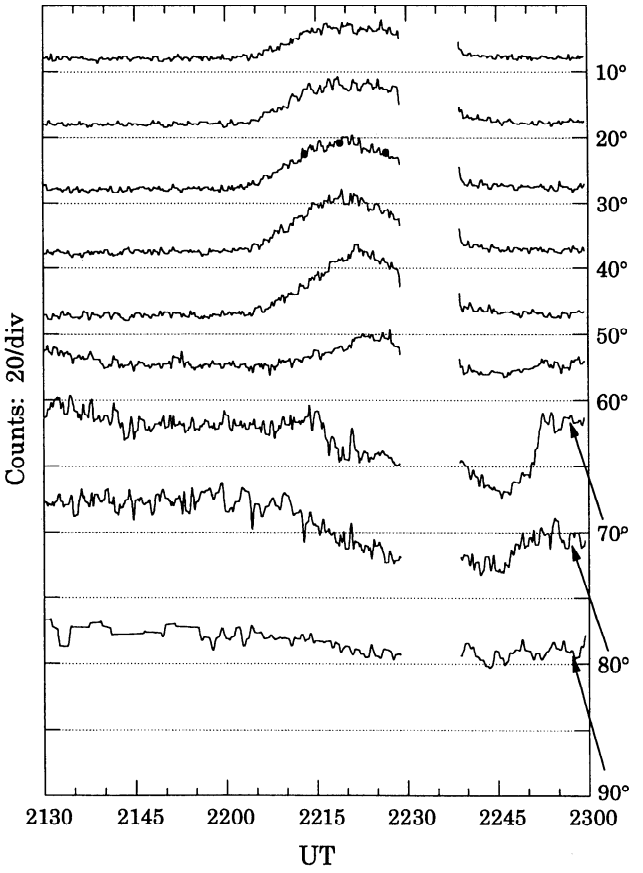

Figure 10a. Ion counts in nine pitch angle bins and in the 56- to 92-keV band for event B (September 17, 1984, day 261). See text for the definition of the three dots on top of the 30° pitch angle trace.

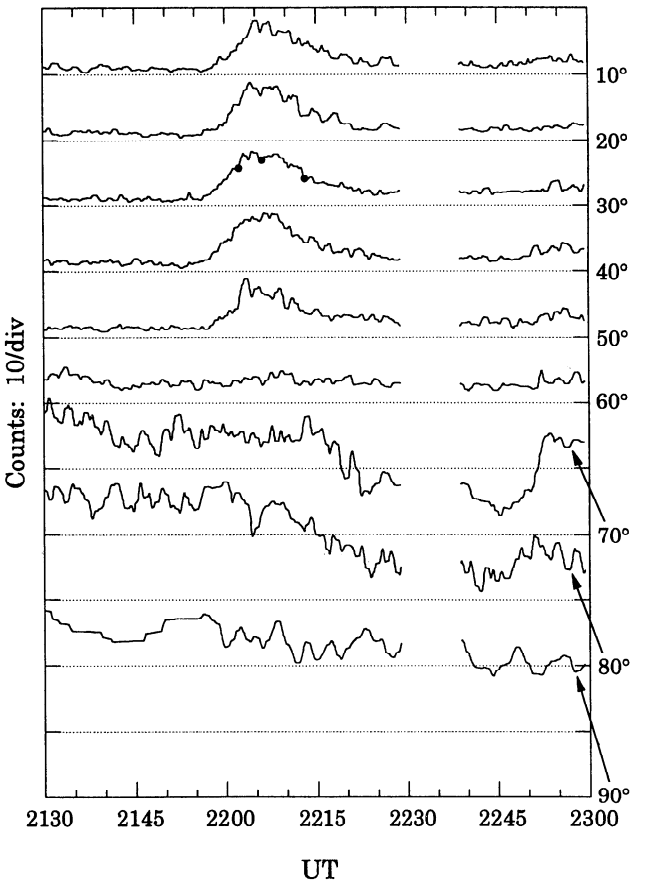

Figure 10b. Same as Figure 10a, except for 92 to 170 keV.

4.2. Detailed Analysis of Event B

To quantify the pitch angle dependence of the injections, we study event B in some detail. This event is chosen because the flux intensity is the highest and it therefore yields the most reliable comparison with the drift calculations. Figures 10a–10c show the pitch angle dependence of ion flux variations in three energy bands. Note that the flux intensity is displayed using a linear scale. For these plots the raw sectored MEPA data were binned into 10° pitch angle bins. The resulting time series in each bin were then smoothed by using 5-point binomial weighting corresponding approximately to a 30-s running average. The pitch angle distribution is assumed to be gyrotropic and symmetric about 90° pitch angles. For example, the 30° bin represents the average of the fluxes for sectors in the pitch angle ranges 25° to 35°, 145° to 155°, 205° to 215°, and 325° to 335°. (The 10° bin corresponds to 0° to 15°, and the 90° bin corresponds to 85° to 95°.) The three dots on the 30° pitch angle trace indicate the calculated arrival times of particles with energies at the minimum, middle, and maximum limits of the energy band and are described in more detail below.

In the 56- to 92-keV band (Figure 10a), a flux enhancement occurred from 2205 to 2240 UT at pitch angles from 10° to 60° (the end time of the flux increase is ambiguous because of the data gap between 2228 and 2239 UT). By contrast, the fluxes in the 70° to 90° bins decrease from 2215 to 2250 UT, and there is no evident increase corresponding to the injection at lower pitch angles. Flux increases for pitch angles lower than 60° are also observed at higher energies, Figures 10b and 10c, with the enhancement occurring earlier at higher energies, indicating that these low pitch angle flux increases are an energy-dispersed injection. The flux decrease in the 70° to 90° bins from 2215 to 2240 UT also occurred at higher energies, but there was no time delay of this signature between different energies. This nondispersive flux decrease occurred simultaneously with a ~7% increase of the magnetic field intensity at CCE. The magnetic field change was likely caused by an increase in the solar wind dynamic pressure, and the flux decrease is attributed to a mirror effect [*Kivelson and Southwood*, 1985] of the ions caused by the local magnetic field change. To summarize the data in Figure 10, energy dispersive injection signatures were observed only at pitch angles below 60°.

Following previous studies using geostationary satellites [*Belian et al.*, 1978; *Reeves et al.*, 1990], we used the energy-time dispersion to estimate the universal time and local time of injection. The T89c Kp = 1 model was used for all comparisons with the event. We first determined the time of flux maximum at 30° pitch angle in the 56- to 92-keV and 92- to 170-keV bands, and from that time traced protons backward in time for the energies at the center of the MEPA energy bands recording the equatorial projection of the instantaneous gyrocenter. The flux maximum is indicated in Figure 10 by a solid dot in the flux trace for 30° pitch angle. The local times of the guiding centers matched at 2149 UT, and at this time the particles were located at 22 MLT. This MLT is reasonable for an injection, and the estimated UT of injection is only 6 min later than the onset of Pi 2 event B. Also shown in Figure 10 are the arrival times of the lower and higher energy limits of each band, indicating that the range of times over which the

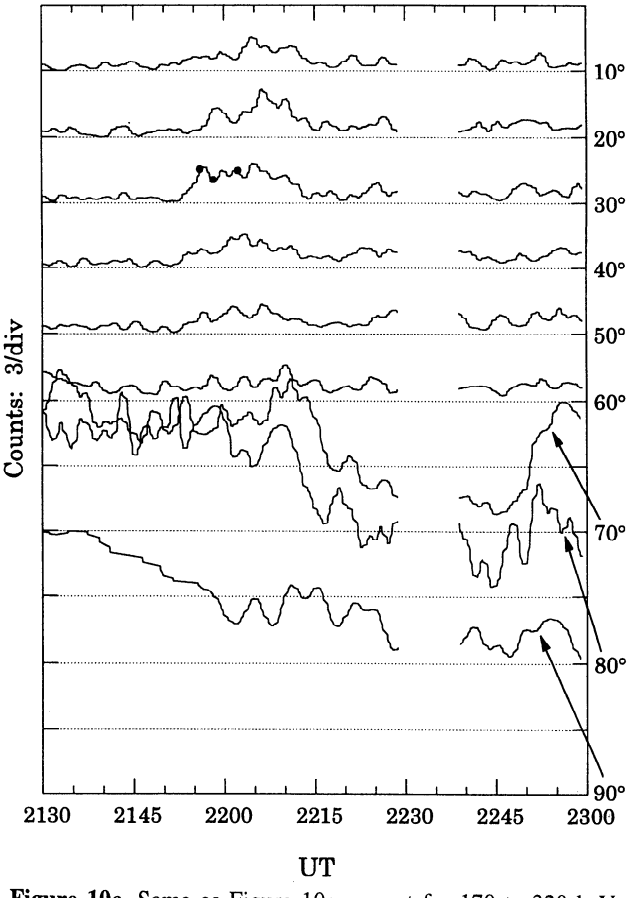

Figure 10c. Same as Figure 10a, except for 170 to 320 keV.

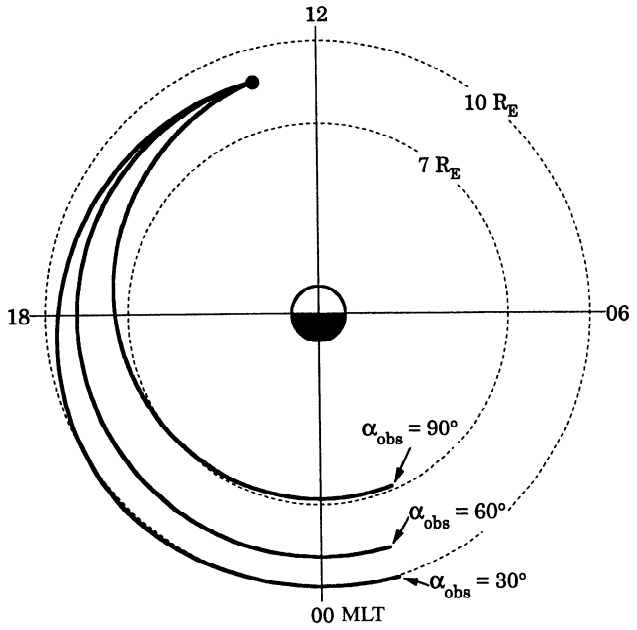

Figure 11. Equatorial intersects of ion orbits calculated for event B for three values of the pitch angle at CCE α_{obs}. The particle energy is assumed to be 200 keV. The orbits were calculated from the CCE location backward in time. The satellite location is indicated by a solid circle.

injection occurs is at least as broad as the energy range of each band.

To check the consistency of the onset location and time estimate, we calculated the drift times for the higher-energy range as well, 170–320 keV (Figure 10c). Using the UT and MLT determined in the above procedure, we calculated the drift time of ions in the 170- to 320-keV energy range between the source point and the satellite. The calculated arrival time of ions with energy at the center (250 keV) of the band is indicated by the center dot above the 30° pitch angle trace. The other two dots are the arrival times for ions with the cutoff energies of 170 and 320 keV. These dots fall in the range of the observed injection, indicating basic consistency with the interpretation of the energy dispersion feature in terms of a remote dispersionless injection.

We interpret the 60° cutoff pitch angle as resulting from an injection having an inner edge, as illustrated in Figure 1. To quantify this interpretation, we show in Figure 11 the numerically calculated guiding center orbits of ions for event B. The format is similar to that of Figure 2, but to facilitate comparison with the event, the observation point is placed at L = 8.7, MLT = 13, and the orbit for α_{obs} = 60° is included. The particle energy, 200 keV, is the same as before. In the local time sector (20–02 MLT) where injections are most likely to occur [*Lopez et al.*, 1990] the drift orbit is nearly circular regardless of pitch angle, and the radii of these orbits are ~10 R_E for α_{obs} = 30°, ~9 R_E for α_{obs} = 60°, and ~7 R_E for α_{obs} = 90°. Therefore, if the injection occurred at 22 MLT, as estimated from the ion energy dispersion, the cutoff pitch angle of α_{obs} = 60° at CCE implies that the inner edge of the injection region was located at about 9 R_E.

4.3. Observations From Geostationary Satellites

The calculated location of the injection inner boundary is consistent with particle observations made at geostationary satellites. Figures 12a and 12b show pitch-angle–averaged charged particle data from three geostationary satellites for the same 5-hour interval as in Figure 8. At geostationary orbit there were no ion (Figure 12a) or electron (Figure 12b) injections at the times of flux enhancements at CCE. Note that ion energies covered by the geosynchronous charged particle analyzers are comparable to those observed by CCE MEPA. Use of the pitch-angle–averaged data is not a serious problem here since two of the spacecraft were located on the nightside. When satellites are close to the source region, drift-shell splitting is small, so injections should be detected at all pitch angles. For the event under study, 1982-019 was in the 18–24 MLT quadrant, a good location for detecting ions drifting westward immediately after they are injected near midnight. Spacecraft 1977-007 was in the 00–06 MLT quadrant, a good location for detecting electrons drifting eastward from the source. Therefore, the absence of injection signatures at these satellites means that injection did not occur at geostationary distance. This leads us to conclude that the ion flux enhancements detected at CCE all occurred at a radial distance greater than 6.6 R_E, as the numerical calculations indicate.

As for the electrons, we do not see any impulsive injections, even at 1977-007 located in the 00–06 MLT quadrant which is ideal for detecting electrons drifting eastward out from the injection region. However, the electron fluxes show a regular small-amplitude oscillation in the 140- to 200-keV channel with a period of ~60 min. This type of electron flux oscillation is common in geosynchronous observations following substorms occurring when the magnetosphere is fairly quiet. The phase of these flux oscillations is different for different energies, but the periods do not match the drift periods, and the dispersion does not regularly increase with time, so they cannot be drift echoes. These oscillations have not been discussed previously in the literature and will be examined in a separate study.

5. Discussion

5.1. Comparison With Ion Injection Boundary Models

The foregoing analyses have shown that observation of injections on the dayside with full pitch angle resolution is useful for estimating the inner boundary of the injection. Previously, inner boundaries have been suggested for substorm injections from different types of particle signatures. *Mauk and McIlwain* [1974] obtained a boundary shape from a statistical analysis of the local time of the encounter of the ATS-5 geostationary satellite with zero-energy particles. The radius of the inner boundary is given as a function of MLT and *Kp* as

$$R_b(\text{ATS-5}) = \frac{122 - 10Kp}{\text{MLT} - 7.3} \quad (1)$$

Note that this boundary shape is for the premidnight sector. The postmidnight portion of the boundary is the mirror image about the midnight meridian of the premidnight boundary.

Lopez et al. [1990] obtained an energetic ion (energy >25 keV) injection boundary using a different approach. They investigated first the spatial occurrence pattern of dispersionless injection events observed with the CCE MEPA instrument and then determined the inner radius limit of the region where dispersionless injections can be observed. The dispersionless events were found only on the nightside from 19 to 06 MLT, unlike the energy-dispersed events in our analysis, indicating that the observations were made within or in close proximity to

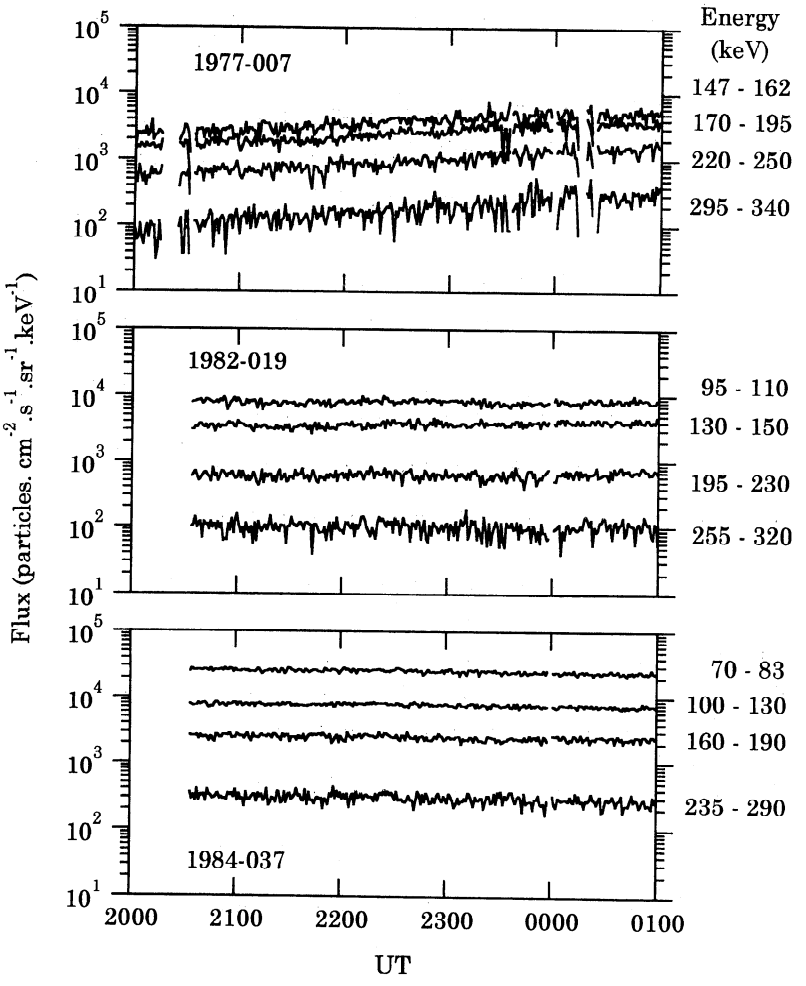

Figure 12a. Los Alamos geostationary CPA ion data from three satellites for the time interval of ion injections observed at CCE (September 17-18, 1984, days 261-262). The data are spin averages and have a time resolution of 10 s.

the region of ion acceleration. *Lopez et al.* [1990] modeled the energetic ion injection boundary using the same functional form as the *Mauk and McIlwain* [1974] boundary. The *Lopez et al.* [1990] boundary is given by

$$R_b(\mathrm{CCE}) = \frac{144 - 17Kp}{\mathrm{MLT} - 10} \qquad (2)$$

As in the case of the *Mauk and McIlwain* [1974] boundary, this boundary is valid only for the premidnight sector, and the boundary for the postmidnight sector is assumed to be the mirror image of (2) about the midnight meridian.

For Kp ~1, appropriate for the interval under study, the above empirical formulas give R_b(ATS-5) ~ 6.7 R_E and R_b(CCE) ~ 9.1 R_E. Our estimate of the inner edge of injection agrees only with the *Lopez et al.* [1990] model. This is not surprising because the two formulas were derived from particle observations at significantly different energies. Because the electric field has a strong control on the drift paths of low-energy ions, it is possible that the detection of low-energy ions at geostationary orbit is the consequence of an earthward convection of the particles after substorm onset. Drift paths of energetic ions, on the other hand, will be dominated by the magnetic field drift, so the particles will drift azimuthally, rather than radially, away from the source region. In the high-energy limit, the drift paths do not depend on the electric field, and the radial distance of the drift orbit of the ions near midnight will be a direct representation of the source location.

Although we discussed only the inner injection boundary, the shell splitting effect might also be useful for detecting a possible outer boundary of injection. One of the major predictions of the current disruption model for substorm onset is that the injection region is initially confined spatially on all sides and then expands both radially outward and in azimuth [*Lopez and Lui*, 1990]. If the injection region is confined within the radial distance range of the nightside drift shells, then the outer injection boundary will produce a cutoff pitch angle on the dayside below which no injection signature is observed. On the particular CCE orbit we studied, there was no indication of such a low pitch angle cutoff, implying that the injection region extended tailward of any of the drift shells of the ions detected at CCE. According to the model ion orbits shown in Figure 11, then, the injection region had an outer edge tailward of 10 R_E.

5.2. Relation of Injection Regions to Substorm Onset Mechanism

Since the earliest substorm studies, it has been known that some substorm onsets develop into global scales, while others do not [*Akasofu*, 1964]. The latter class of onsets is referred to as pseudobreakups or pseudo-substorm onsets. In the September

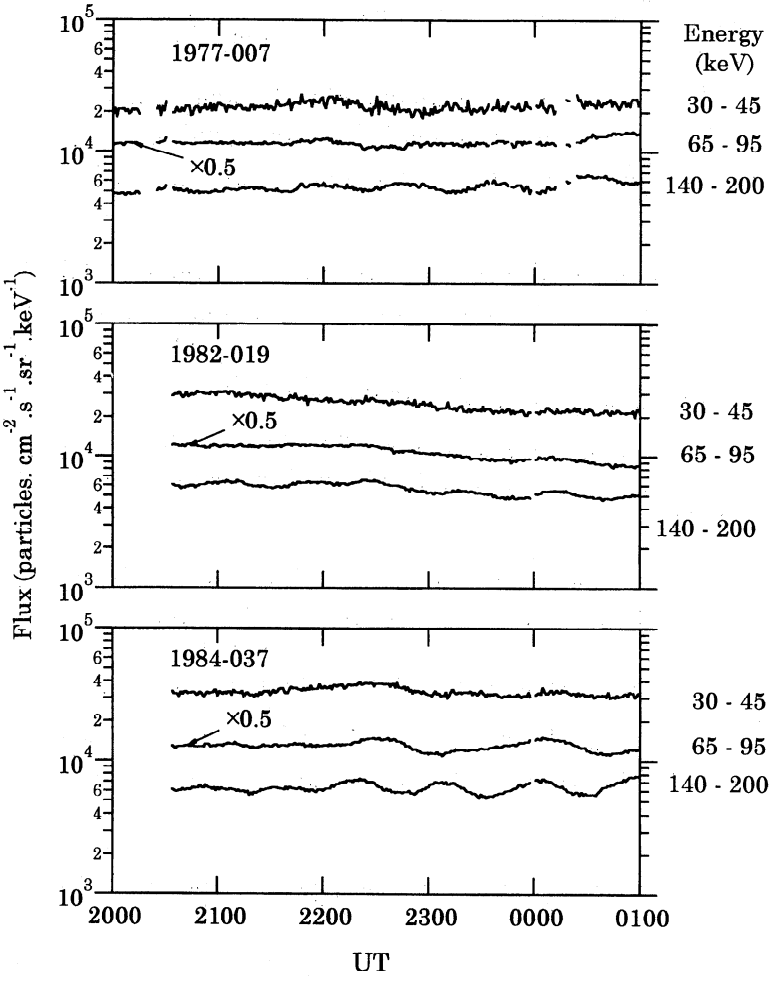

Figure 12b. Los Alamos geostationary CPA electron data from three satellites for the time interval of ion injections observed at CCE (September 17-18, 1984, days 261-262). The data are spin averages and have a time resolution of 10 s.

17, 1984, event, no clear injection signature was observed at geosynchronous altitude in the midnight sector, and the amplitude of the negative bay in the auroral zone was very small. We therefore interpret the event as an example of a pseudobreakup.

Recently, several attempts were made to distinguish pseudo-substorm onsets from standard substorm onsets in terms of the near-Earth substorm process [*Koskinen et al.*, 1993; *Ohtani et al.*, 1993; *Nakamura et al.*, 1994]. *Koskinen et al.* [1993] reported an event in which an extremely weak injection signature was observed by a LANL geosynchronous satellite in the midnight sector. *Ohtani et al.* [1993] also found the absence of a clear depolarization signature at geosynchronous altitude for a pseudo-substorm onset event. In both events, CCE was located about 2 R_E outward of geosynchronous altitude and observed typical dipolarization and injection signatures, suggesting that the acceleration region was located tailward of the geosynchronous orbit. In addition, the acceleration region may be highly localized in the azimuthal direction, as suggested by *Nakamura et al.* [1994].

Considering that injection and dipolarization signatures are rather common in the geosynchronous region for global substorms, the absence of such signatures in those pseudo-substorm onset events suggests that the acceleration of particles tends to occur at a larger geocentric distance when the intensity of substorms is weaker. There is some evidence that supports this idea. *Akasofu* [1964] found that the global auroral expansion initiates at the most equatorward arc, whereas pseudo-substorm onsets (pseudobreakups) tend to take place during the growth phase at an auroral arc other than the most equatorward one. Although one cannot accurately map the nightside auroral zone to the equatorial plane, the tendency of pseudo-onset auroral forms to occur poleward of full-fledged breakup onsets is consistent with our interpretation. In a related study, *Singer et al.* [1983] found that Pi 2 signatures are observed less often at synchronous altitude than on the ground during periods of low magnetic activity, even if the spacecraft is located in the midnight sector. From this result they suggested that substorm signatures at synchronous altitude depend on the radial distance of onset regions, which are located at large distances.

The occurrence of pseudo-substorm onsets farther out from the Earth may be explained in terms of the tail magnetic configuration [*Ohtani et al.*, 1993]. For quiet conditions the enhancement in the tail current intensity is presumably weak, so that its effect is not significant in the geosynchronous region. It is therefore likely that the transition from the dipole to taillike magnetic field configurations occurs farther out from the Earth before pseudo-substorm onsets than before standard substorm

onsets. If substorms are triggered in such a magnetic configuration (Kiruna conjecture [*Kennel*, 1992]), this idea is consistent with the result of the previous observations.

The present study suggests that one must consider the effects of drift-shell splitting and the resulting pitch angle distributions of injected ions to avoid confusing the longitudinal and radial structure of the source region when interpreting particle injection data recorded beyond geosynchronous orbit. Moreover, the results indicate that we can use the measurement of dayside injection signatures to remotely sense the radial structure of the injection region.

6. Conclusions

We studied energetic ion injection events associated with a series of pseudo-substorm onsets using data acquired by the AMPTE/CCE spacecraft in the dayside magnetosphere. The primary emphasis of our analysis was on the pitch angle dependence of injection signatures. The flux enhancement signatures were observed only below a certain cutoff pitch angle.

This pitch angle dependence is interpreted in terms of the drift-shell splitting effect. The degree of shell splitting was evaluated using a realistic magnetic field model and calculation of the ion drift orbits. It was found that the ions that reach a single observing point on the dayside at 8.5 R_E with a full range of pitch angles have nightside drift shells ranging from ~6.5 to ~10 R_E in equatorial geocentric distance. This geometric property of drifting ions makes it possible to use the energetic ions to remotely sense the radial boundaries of substorm injections. For the pseudo-onset–associated event studied in detail, we estimate that the injection inner boundary was located at ~9 R_E.

Previously, energy dispersive features of energetic particles were extensively used to identify the location and timing of injections on the nightside. Our study demonstrates that pitch angle–resolved energetic ion data, in particular those acquired away from the location of injections and at distances beyond geosynchronous orbit, provide valuable information on the radial location of particle energization associated with substorms. This feature of the particles, when combined with previously used in situ and remote sensing techniques, will be a useful tool in studying substorms.

Acknowledgments. We are grateful to the AMPTE/CCE Science Team and Science Data Center for providing AMPTE/CCE energetic particle data and to T. Iyemori of Kyoto University World Data Center for providing Wingst magnetograms. Work at The Johns Hopkins University Applied Physics Laboratory (JHU/APL) was supported by NASA through Grant NAGW-4133, NSF, and Office of Naval Research. One of the authors (K. T.) is grateful to Larry Zanetti for making his research at JHU/APL possible. Work at Los Alamos National Laboratory was supported by the Department of Energy Office of Basic Energy Science.

The editor thanks S. W. H. Cowley and another referee for their assistance in evaluating this paper.

References

Akasofu, S.-I., The development of the auroral substorm, *Planet. Space Sci., 12*, 273–282, 1964.

Anderson, B.J., R.B. Decker, N.P. Paschalidis, and T. Sarris, Onset of nonadiabatic particle motion in the nearEarth magnetotail, *J. Geophys. Res., 102*, 17,553-17,569, 1997.

Baker, D. N., R. D. Belian, P. R. Higbie, and E. W. Hones Jr., High-energy magnetospheric protons and their dependence on geomagnetic and interplanetary conditions, *J. Geophys. Res., 84*, 7138–7154, 1979.

Belian, R. D., D. N. Baker, P. R. Higbie, and E. W. Hones Jr., High-resolution particle measurements at 6.6 R_E 2: High-energy proton drift echoes, *J. Geophys. Res., 83*, 4857–4862, 1978.

Belian, R. D., D. N. Baker, E. W. Hones Jr., and P. R. Higbie, High-energy proton drift echoes: Multiple peak structure, *J. Geophys. Res., 89*, 9101–9106, 1984.

Birmingham, T. J., Pitch angle diffusion in the Jovian magnetodisc, *J. Geophys. Res.*, 89, 2699–2707, 1984.

Brewer, H. R., M. Schultz, and A. Eviatar, Origin of drift-periodic echoes in outer-zone electron flux, *J. Geophys. Res., 74*, 159–167, 1969.

DeForest, S. E., and C. E. McIlwain, Plasma clouds in the magnetosphere, *J. Geophys. Res., 76*, 3587–3611, 1971.

Ejiri, M., R. A. Hoffman, and P. H. Smith, Energetic particle penetrations into the inner magnetosphere, *J. Geophys. Res., 85*, 653–663, 1980.

Fairfield, D. H., Trapped particles in a distorted dipole field, *J. Geophys. Res., 69*, 3919–3926, 1964.

Friedel, R. H. W., A. Korth, and G. Kremser, Substorm onsets observed by CRRES: Determination of energetic particle source regions, *J. Geophys. Res., 101*, 13,137–13,154, 1996.

Hones, E. W. Jr., Motion of charged particles trapped in the Earth's magnetosphere, *J. Geophys. Res., 68*, 1209–1219, 1963.

Kennel, C., The Kiruna Conjecture: The strong version, in *Proceedings of the International Conference on Substorms (ICS-1), Eur. Space Agency Spec. Publ., ESA SP-335*, 599, 1992.

Kivelson, M. G., and D. J. Southwood, Charged particle behavior in low-frequency geomagnetic pulsations, 4, Compressional waves, *J. Geophys. Res., 90*, 1486–1498, 1985.

Konradi, A., Proton events in the magnetosphere associated with magnetic bays, *J. Geophys. Res., 72*, 3829–3841, 1967.

Konradi, A., C. L. Semar, and T. A. Fritz, Substorm-injected protons and electrons and the injection boundary model, *J. Geophys. Res., 80*, 543–552, 1975.

Koskinen, H. E., R. E. Lopez, R. J. Pellinen, T. I. Pulkkinen, D. N. Baker, and T. Bosinger, Pseudobreakup and substorm growth phase in the ionosphere and magnetosphere, *J. Geophys. Res., 98*, 5801–5813, 1993.

Lanzerotti, L. J., C. G. Maclennan, and M. F. Robins, Proton drift echoes in the magnetosphere, *J. Geophys. Res., 76*, 259–263, 1971.

Lopez, R. E., and A. T. Y. Lui, A multisatellite case study of the expansion of a substorm current wedge in the near-Earth magnetotail, *J. Geophys. Res., 95*, 8009–8017, 1990.

Lopez, R. E., D. G. Sibeck, R. W. McEntire, and S. M. Krimigis, The energetic ion substorm injection boundary, *J. Geophys. Res., 95*, 109–117, 1990.

Lühr, H., S. Thürey, and N. Klöcker, 1984: The EISCAT magnetometer cross, *Geophys. Surv., 6*, 305–315, 1984.

Mauk, B. H., and C. E. McIlwain, Correlation of *Kp* with the substorm-injected plasma boundary, *J. Geophys. Res., 79*, 3193–3196, 1974.

Maynard, N. C., and A. J. Chen, Isolated cold plasma regions: Observations and their relation to possible production mechanisms, *J. Geophys. Res., 80*, 1009–1013, 1975.

McEntire, R. W., E. P. Keath, D. E. Fort, A. T. Y. Lui, and S. M. Krimigis, The Medium-Energy Particle Analyzer (MEPA) on the AMPTE CCE spacecraft, *IEEE Trans. Geosci. Remote Sens., GE-23*, 231–233, 1985.

McIlwain, C. E., Substorm injection boundaries, in *Magneto-*

spheric Physics, edited by B. M. McCormac, p. 143, D. Reidel, Norwell, Mass., 1974.

Nakamura, R., D. N. Baker, T. Yamamoto, R. D. Belian, E. A. Bering, J. R. Benbrook, and J. R. Theall, Particle and field signatures during pscudobreakup and major expansion onset, *J. Geophys. Res., 99*, 207–221, 1994.

Ohtani, S., et al., A multisatellite study of a pseudo-substorm onset in the near-Earth magnetotail, *J. Geophys. Res., 98*, 19,355–19,367, 1993.

Peredo, M., D. P. Stern, and N. A. Tsyganenko, Are existing magnetospheric models excessively stretched?, *J. Geophys. Res., 98*, 15,343–15,354, 1993.

Reeves, G., D., T. A. Fritz, T. E. Cayton, and R. D. Belian, Multisatellite measurements of the substorm injection region, *Geophys. Res. Lett., 17*, 2015–2018, 1990.

Reeves, G. D., R. D. Belian, and T.A. Fritz, Numerical tracing of energetic particle drifts in a model magnetosphere, *J. Geophys. Res., 96*, 13,997–14,008, 1991.

Roederer, J. G., On the adiabatic motion of energetic particles in a model magnetosphere, *J. Geophys. Res., 72*, 981–992, 1967.

Singer, H. J., W. J. Hughes, P. D. Fougere, and D. J. Knecht, The localization of Pi 2 pulsations: Ground-satellite observations, *J. Geophys. Res., 88*, 7029–7036, 1983.

Speiser, T. W., Particle trajectories in model current sheets, 1, Analytical solutions, *J. Geophys. Res., 70*, 4219–4226, 1965.

Stern, D. P., The motion of a proton in the equatorial magnetosphere, *J. Geophys. Res., 80*, 595–599, 1975.

Takahashi, S., and T. Iyemori, Three-dimensional tracing of charged particle trajectories in a realistic magnetospheric model, *J. Geophys. Res., 94*, 5505–5509, 1989.

Tsyganenko, N. A., A magnetospheric magnetic field model with a warped tail current sheet, *Planet. Space Sci., 37*, 5–20, 1989.

Tsyganenko, N. A., and A. V. Usmanov, Determination of the magnetospheric current system parameters and development of experimental geomagnetic field models based on data from IMP and HEOS satellites, *Planet. Space Sci., 30*, 985–998, 1982.

Volland, H., A semiempirical model of large-scale magnetospheric electric fields, *J. Geophys. Res., 78*, 171–180, 1973.

Walker, R. J., K. N. Erickson, and J. R. Winkler, Pitch angle dispersion of drifting energetic protons, *J. Geophys. Res., 83*, 1595–1600, 1978.

B. J. Anderson and S. Ohtani, Applied Physics Laboratory, The Johns Hopkins University, Johns Hopkins Road, Laurel, MD 20723-6099. (e-mail: anderson@ampvx2.jhuapl.edu; ohtani@slpvx4.jhuapl.edu)

K. Mursula, Department of Physical Sciences, University of Oulu, POB 400, FIN-90571 Oulu, Finland. (e-mail: kalevi.mursula@oulu.fi)

G. D. Reeves, Los Alamos National Laboratory, MD D436, Los Alamos, NM 87545. (e-mail: reeves@lanl.gov)

T. E. Sarris, Department of Physics, University of Athens, Athens (ZograFou, 16232), Greece (e-mail: cc@xansrc.ee.duth.gr)

K. Takahashi, Solar-Terrestrial Environment Laboratory, Nagoya University, Toyokawa, Aichi 442, Japan. (e-mail: kazue@stelab.nagoya-u.ac.jp)

S. Takahashi, Power and Industrial R&D Division, Hitachi Ltd., Hitachi, Ibaraki 319-12, Japan. (e-mail: shunchan@erl.hitachi.co.jp)

(Received February 10, 1997; revised June 11, 1997; accepted June 19, 1997.)